Pergamon

Int. J. Solids Structures Vol. 35, No. 13, pp. 1325–1338, 1998

0020–7683/98 $19.00 + .00

PII: S0020–7683(97)00094–2

THE CONTROL VOLUME FINITE ELEMENT NUMERICAL SOLUTION TECHNIQUE APPLIED TO CREEP IN SOFTWOODS

W. J. FERGUSON

Division of Civil Engineering, Cardiff School of Engineering, University of Wales, Cardiff, Queen's Buildings, PO Box 917, Newport Road, Cardiff, CF2 1XH, U.K.

(*Received* 18 *January* 1996; *in revised form* 4 *April* 1997)

Abstract—This paper presents the novel application of the control volume finite element method (CVFE), otherwise known as the vertex-centered control volume scheme, to creep problems. The discretisation procedure is valid for both structured and unstructured meshes thus enabling complex geometries to be modelled. Analytical solutions to engineering problems involving creep often do not exist, therefore, a comparison with the well established numerical solution technique, the finite element method, has been included to provide a benchmark solution. © 1998 Elsevier Science Ltd.

INTRODUCTION

Materials often exhibit a long-term behaviour which is different to that defined by elasto-plastic theories which model the instantaneous time-independent response. Consider the case where a bar is subjected to a constant load. The initial response of the bar is to deform elastically, developing internal forces required to support the load. Over an extended period of time, the bar will continue to deform, without an increase in the applied load, which may eventually result in rupture or ultimate failure. This time-dependent behaviour is known as creep.

Analytical solutions exist in only the simplest of cases. Most engineering problems are comprised of complex geometries and loading configurations making an analytical solution impossible. In order to achieve a solution, a numerical solution technique must be employed. Over the past 25 years, the finite element method (FE) has been utilised successfully to predict stress/strain distributions associated with materials under thermal and mechanical loadings, Zienkiewicz and Cormeau (1974) and Duxbury *et al.* (1994). In the past, control volume techniques have struggled against the finite element method due to their reliance upon structured meshes, Patankar (1980), and, hence, have been perceived as disadvantaged when modelling complex shapes.

Two control volume, or finite volume, methods exist. The most common is the cell-centred approach which requires that a rectangular grid be employed. Recently, Turner and Ferguson (1995a, 1995b) developed a variation of the cell-centred scheme which enabled polygonal cells of any order to be utilised, thus enabling complex geometrical shapes to be meshed.

The second control volume method was first proposed by Patankar (1980) and is a hybrid of the cell-centred approach and the finite element method. This scheme is known as the vertex-centred control volume method or alternatively as the control volume finite element method (CVFE). Control volumes are constructed about the modal points of a finite element mesh, which is used solely for the interpolation of the system variables within the computational domain. Linear triangular or quadrilateral elements are used in the background interpolation grid giving rise to high ordered cells in the control volume computational grid. High ordered cells, in relation to the control volume method, are control volumes with a large number of faces which in turn increases the accuracy of the mass, energy or force balance across the boundary of the control volume. Ferguson and

Turner (1995a) compared the two control volume schemes and concluded that the vertex-centred was the more accurate for an anisotropic material due to the interpolating functions employed.

The CVFE method has been employed in fields as diverse as reservoir modelling, Fung *et al.* (1992), casting problems, Bailey *et al.* (1993), and elasticity, Bailey *et al.* (1995), Taylor *et al.* (1995) and Onate *et al.* (1994). This paper presents the novel application of the control volume finite element method to creep problems. The discretisation procedure is described in detail and is applicable to both structured and unstructured meshes without alteration to the formulation. Two practical creep problems are solved, firstly for a beam for which an analytic solution exists, and secondly for drying stresses in timber. A finite element solution is employed in both numerical examples purely as a benchmark in order to ascertain the validity of the CVFE solution and to ensure that the correct solution characteristics are obtained.

CREEP MODEL

A tensile specimen under a constant stress will deform with time, this phenomenom is known as *creep*. This deformation depends on three main parameters, stress, time and temperature. A general creep equation can be written as

$$\varepsilon_c = f(\sigma, t, T). \tag{1}$$

A useful approximation is to limit this general function to a commutative law of the form

$$\varepsilon_c = f_1(\sigma) f_2(t) f_3(T). \tag{2}$$

The separation of the functions $f_1(\sigma)$, $f_2(t)$ and $f_3(T)$ has been implicit in most of the previously published work and first emerged during early studies of secondary creep by Andrade (1910) and McVetty (1934, 1943).

The stress-strain relationship for creep problems in timber, Ranta-Maunus (1975), can be written as,

$$\frac{\partial \varepsilon}{\partial t} = \frac{1}{E}\frac{\partial \sigma}{\partial t} + (\alpha + m\sigma)\frac{\partial \phi}{\partial t} \tag{3}$$

where E and α represent Young's modulus and the coefficient of free shrinkage respectively and ϕ generally denotes temperature. The stress σ and strain ε vectors are given by $(\sigma_{xx}, \sigma_{yy}, \Gamma_{xy})^T$, respectively. In timber drying, creep is known to be a function of the bound water X_{wb} and in this case $\phi = X_{wb}$. The bound water X_{wb} is the moisture in the porous medium that is hygroscopically held to the cell walls. This type of creep is referred to as *mechano-sorptive* creep. Equation 3 can be integrated with respect to time to give the following equation for total strain, Ranta-Maunus (1975),

$$\varepsilon = \frac{1}{E}\sigma + \alpha\Delta\phi + \int_t^{t+\Delta t} m\sigma \frac{\partial \phi}{\partial t}\,\mathrm{d}\tau \tag{4}$$

$$= \frac{1}{E}\sigma + \alpha\Delta\phi + m\sigma\Delta\phi \tag{5}$$

where

$$\Delta\phi = \phi^{n+1} - \phi^n. \tag{6}$$

The superscripts $n+1$ and n denote the current and previous timesteps, respectively. If the creep coefficient m equals zero, the constitutive equation reduces to stress-strain law for an

elastic material. Equation 5 states that the total strain is the sum of the components of elastic strain ε_e, free shrinkage strain ε_{fs} and strain due to creep ε_c such that

$$\varepsilon = \varepsilon_e + \varepsilon_{fs} + \varepsilon_c. \tag{7}$$

If the free shrinkage and creep components of strain are modelled as initial strains, Zienkiewicz and Cormeau (1974), i.e. $\varepsilon_o = \varepsilon_{fs} + \varepsilon_c$, then the two-dimensional stress-strain relationship is given by

$$\boldsymbol{\sigma} = \mathbf{D}(\boldsymbol{\varepsilon} - \boldsymbol{\varepsilon}^o) + \boldsymbol{\sigma}^o \tag{8}$$

where

$$\boldsymbol{\sigma} = \begin{Bmatrix} \sigma_{xx} \\ \sigma_{yy} \\ \Gamma_{xy} \end{Bmatrix} \quad \boldsymbol{\sigma}^o = \begin{Bmatrix} \sigma^o_{xx} \\ \sigma^0_{yy} \\ \Gamma^o_{xy} \end{Bmatrix} \quad \boldsymbol{\varepsilon} = \begin{Bmatrix} \varepsilon_{xx} \\ \varepsilon_{yy} \\ \gamma_{xy} \end{Bmatrix} \tag{9}$$

and for *plane stress* problems,

$$\boldsymbol{\varepsilon}^o = \begin{Bmatrix} \varepsilon^0_{xx} \\ \varepsilon^0_{yy} \\ \gamma^0_{xy} \end{Bmatrix} = \begin{Bmatrix} (\alpha + m\sigma_{xx})\Delta\phi \\ (\alpha + m\sigma_{yy})\Delta\phi \\ 0 \end{Bmatrix} \tag{10}$$

and for *plane strain* problems,

$$\boldsymbol{\varepsilon}^o = \begin{Bmatrix} \varepsilon^0_{xx} \\ \varepsilon^0_{yy} \\ \gamma^0_{xy} \end{Bmatrix} = \begin{Bmatrix} (1+v)(\alpha + m\sigma_{xx})\Delta\phi \\ (1+v)(\alpha + m\sigma_{yy})\Delta\phi \\ 0 \end{Bmatrix}. \tag{11}$$

Poisson's ratio is denoted by vi and $\boldsymbol{\sigma}^o$ represents the initial stress. The terms which comprise the matrix **D** can be found in Zienkiewicz (1977). Modelling the creep term as an initial strain enables the *initial strain* method, Zienkiewicz (1977), to be employed. In this manner the incremental stresses and strains can be evaluated throughout the computational domain for every timestep. The initial strain at the start of the timestep $\boldsymbol{\varepsilon}^o$ is a function of the total stresses $\boldsymbol{\sigma}$ at the end of the timestep, implying that an iterative procedure should be utilised to account for the non-linearity. Zienkiewicz and Cormeau (1974) state that for most practical problems the incurred error, by taking $\boldsymbol{\sigma}$ as the stress distribution at the start of the timestep, is negligible.

CVFE DISCRETISATION

For two-dimensional plane stress or plane strain problems the following mechanical equilibrium equations apply at each point within the solid where there are no internal body forces applied.

$$\frac{\partial \sigma_{xx}}{\partial x} + \frac{\partial \Gamma_{xy}}{\partial y} = 0 \tag{12}$$

$$\frac{\partial \Gamma_{xy}}{\partial x} + \frac{\partial \sigma_{yy}}{\partial y} = 0. \tag{13}$$

Integrating eqns 12 and 13 using Green's theorem across any control volume boundary yields,

$$\oint_c (\sigma_{xx}\,dy - \Gamma_{xy}\,dx) = 0 \tag{14}$$

$$\oint_c (\Gamma_{xy}\,dy - \sigma_{yy}\,dx) = 0. \tag{15}$$

The relationship between stress and strain given in eqn 8 can be written as,

$$\begin{aligned}
\sigma_{xx} &= D_{11}\varepsilon_{xx} + D_{12}\varepsilon_{yy} - D_{11}\varepsilon^o_{xx} - D_{12}\varepsilon^o_{yy} \\
\sigma_{yy} &= D_{21}\varepsilon_{xx} + D_{22}\varepsilon_{yy} - D_{21}\varepsilon^o_{xx} - D_{22}\varepsilon^o_{yy} \\
\Gamma_{xy} &= D_{33}\gamma_{xy} - D_{33}\gamma^o_{xy}.
\end{aligned} \tag{16}$$

The strains can be written in terms of the derivatives of the x and y components of the displacements u and v, respectively,

$$\varepsilon_{xx} = \frac{\partial u}{\partial x} \quad \varepsilon_{yy} = \frac{\partial v}{\partial y} \quad \varepsilon_{xy} = \frac{\partial v}{\partial x} + \frac{\partial u}{\partial y}. \tag{17}$$

Substituting eqns 16 and 17 into eqn 14 gives,

$$\oint_c D_{11}\,dy\frac{\partial u}{\partial x} + D_{12}\,dy\frac{\partial v}{\partial y} - D_{33}\,dx\frac{\partial u}{\partial y} - D_{33}\,dx\frac{\partial v}{\partial x} - D_{11}\,dy\varepsilon^0_{xx} - D_{12}\,dy\varepsilon^o_{yy} + D_{33}\,dx\gamma^o_{xy} = 0. \tag{18}$$

The control volume computational grid is constructed from a finite element mesh by connecting the centroid of each element to the midpoint of the element faces, Fig. 1. Each

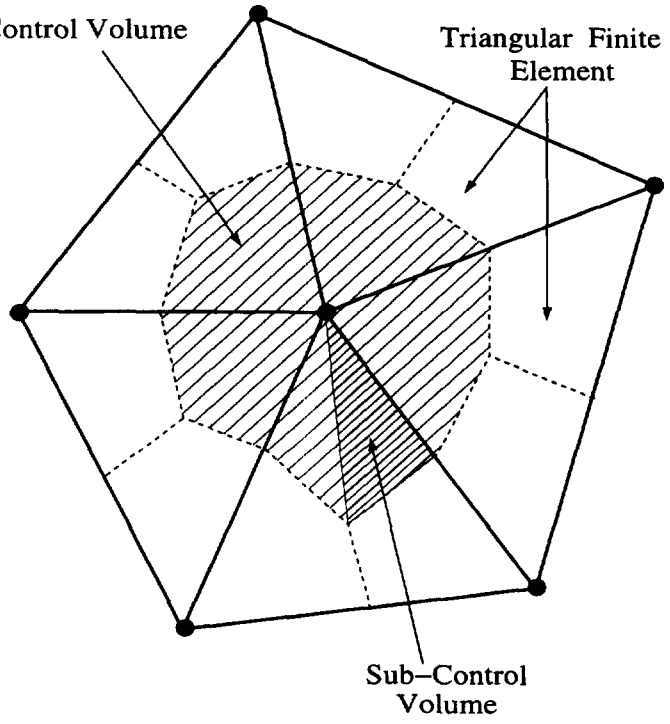

Fig. 1. Construction of control volume mesh from interpolation grid.

finite element contributes two sub-control volumes to the control volume, which may be either convex or concave. The finite element nodes are assumed to be the representative points of the control volumes. The finite element mesh can be viewed as a background or interpolation grid which is utilised solely to evaluate the system variables at the midpoint of the control volume faces. Any variable within an element can be defined in terms of the nodal values, Zienkiewicz (1977), as follows,

$$\Phi \approx \sum_{i=1}^{3} N_i \Phi_i \tag{19}$$

where N_i denotes the standard finite element shape or basis functions. The derivatives of any variable, with respect to x and y, can be approximated within the element in the same manner as the variable itself, such that

$$\frac{\partial \Phi}{\partial x} = \sum_{i=1}^{3} \frac{\partial N_i}{\partial x} \Phi_i \quad \frac{\partial \Phi}{\partial y} = \sum_{i=1}^{3} \frac{\partial N_i}{\partial y} \Phi_i. \tag{20}$$

Summing around the control volume and substituting the finite element approximations to the global derivatives, eqn 20, into eqn 18 gives,

$$\sum_{i=1}^{nscv} \sum_{j=1}^{nvert} D_{11} \Delta y_{ij} \frac{\partial N_j}{\partial x} u_j + D_{12} \Delta y_{ij} \frac{\partial N_j}{\partial y} v_j - D_{33} \Delta x_{ij} \frac{\partial N_j}{\partial y} u_j - D_{33} \Delta x_{ij} \frac{\partial N_j}{\partial x} v_j$$
$$- D_{11} \Delta y_{ij} \varepsilon_{xx}^o - D_{12} \Delta y_{ij} \varepsilon_{yy}^o + D_{33} \Delta x_{ij} \gamma_{xy}^o = 0. \tag{21}$$

The same procedure is followed for eqn 15 to yield the final discretised form,

$$\sum_{i=1}^{nscv} \sum_{j=1}^{nvert} D_{33} \Delta y_{ij} \frac{\partial N_j}{\partial y} u_j + D_{33} \Delta y_{ij} \frac{\partial N_j}{\partial x} v_j - D_{21} \Delta x_{ij} \frac{\partial N_j}{\partial x} u_j - D_{22} \Delta x_{ij} \frac{\partial N_j}{\partial y} v_j$$
$$- D_{33} \Delta y_{ij} \gamma_{xy}^o - D_{21} \Delta x_{ij} \varepsilon_{xx}^o + D_{22} \Delta x_{ij} \varepsilon_{yy}^o = 0 \tag{22}$$

where *nscv* is the number of sub-control volumes, *nvert* is the number of vertices of the finite element and Δx and Δy are the lengths of the components of the control volume face in the x and y directions, respectively.

Equations 21 and 22 can be constructed for every representative point, i.e. the nodal points on the finite element background grid, in the computational mesh to yield a system of equations which can be written as

$$\mathbf{K}\boldsymbol{\delta} = \mathbf{F} \tag{23}$$

where $\mathbf{K}$ denotes the *stiffness* matrix, $\mathbf{F}$ the *force* vector and $\boldsymbol{\delta}$ the displacements in the x and y directions for each point. The system of equations was solved using GMRES, with a block ILU preconditioner, for the displacements $\boldsymbol{\delta}$, from which the incremental strains and stresses can be determined.

FINITE ELEMENT DISCRETISATION

The common starting point in all finite element analysis is the principle of virtual work equilibrium equation. Consider a single element acted upon by nodal loads $\mathbf{F}^e$ and body forces $\mathbf{p}$ which result in an equilibrating stress field $\boldsymbol{\sigma}$, then the principle of virtual work equilibrium equation becomes,

$$\int_{V^e} \mathbf{B}^T \boldsymbol{\sigma} \, \mathrm{d}V = \int_{V^e} \mathbf{N}^T \mathbf{p} \, \mathrm{d}V + \mathbf{F}^e. \tag{24}$$

Substituting for $\boldsymbol{\sigma}$ from eqn 8 and assuming that neither nodal loads nor body forces are applied, then

$$\left\{ \int_{V^e} \mathbf{B}^T \mathbf{D} \mathbf{B} \, \mathrm{d}V \right\} \boldsymbol{\delta}^e = \int_{V^e} \mathbf{B}^T \mathbf{D} \boldsymbol{\varepsilon}^o \, \mathrm{d}V - \int_{V^e} \mathbf{B}^T \boldsymbol{\sigma}^o \, \mathrm{d}V \tag{25}$$

where $\mathbf{B}$ is termed the *strain matrix* and is given by

$$\mathbf{B}_i = \begin{bmatrix} \dfrac{\partial N_i}{\partial x} & 0 \\ 0 & \dfrac{\partial N_i}{\partial y} \\ \dfrac{\partial N_i}{\partial y} & \dfrac{\partial N_i}{\partial x} \end{bmatrix} \quad \text{and where } \boldsymbol{\varepsilon} = \mathbf{B}\boldsymbol{\delta}^e = \sum_{i=1}^{n} \mathbf{B}_i \boldsymbol{\delta}_i. \tag{26}$$

Equation 25 can be written in the form:

$$\mathbf{K}^e \boldsymbol{\delta}^e = \mathbf{F}^e_{\varepsilon^o} + \mathbf{F}^e_{\sigma^o} \tag{27}$$

where $\mathbf{K}^e$ represents the *element* stiffness matrix and $\mathbf{F}^e_{\varepsilon^o}$ and $\mathbf{F}^e_{\sigma^o}$ represent the initial strain and initial stress loadings. Equation 27 is only true if one element is considered. In general, the *global* stiffness matrix and force vector are obtained by summing the elemental forms for all elements in the structure, which can then be solved for the nodal displacements. The element stresses can then be obtained from the relation

$$\boldsymbol{\sigma} = \mathbf{D}(\mathbf{B}\boldsymbol{\delta}^e - \boldsymbol{\varepsilon}^o) + \boldsymbol{\sigma}^o. \tag{28}$$

The finite element formulation has been previously been well-documented, hence, only a brief description has been presented here, and further details can be found in Zienkiewicz (1977).

NUMERICAL RESULTS AND DISCUSSION

Two creep problems are solved numerically to highlight the advantages, disadvantages and differences between the finite element method and the control volume finite element. Firstly, a beam is subjected to a known variation in both space and time which yields a one-dimensional stress distribution for which an analytical solution can be found, against which the numerical solutions are compared. The second example considers a more realistic engineering problem whereby the drying stresses in timber are calculated. In this case, mechano-sorptive creep is considered which is a function, not of the temperature change, but of the change in moisture content as the convective drying process advances in time.

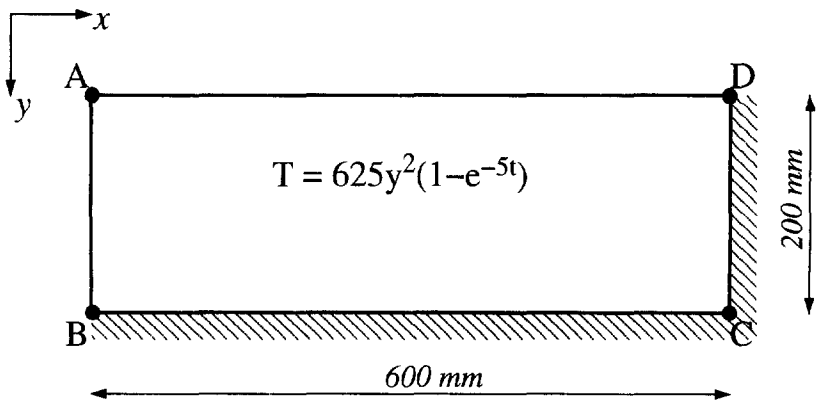

Fig. 2. Cross-section through cantilever.

Thermal problem

The beam under consideration, Fig. 2, has dimensions 600 mm × 200 mm in the x and y directions, respectively. Initially ($t = 0$ hrs) the temperature of the material is 0°C which varies in both space and time as,

$$T(y, t) = 625y^2(1 - e^{-5t}). \tag{29}$$

The applied temperature variation is one-dimensional in order to gain an analytical solution, Boley and Weiner (1960), to the problem. The beam is restrained in the x direction on face CD and in the y direction on face BC, point C is fixed in both the x and y directions. Material properties of the beam are Young's Modulus $E = 5 \times 10^7$ Pa, coefficient of thermal expansion $\alpha = 0.01°C^{-1}$, Poisson's ratio $\nu = 0.25$ and the creep coefficient $m = 0.05 \times 10^{-7}$ Pa^{-1}. Plane stress is assumed.

The finite element mesh of the computational domain, Fig. 2 ABCD, is comprised of linear triangular elements with the total number of nodal points ranging from 60 to 2250. A typical mesh is shown in Fig. 3. The control volume finite element mesh is constructed from the finite element mesh, which is utilised as an interpolation grid, and is shown in Fig. 4. The control volumes in Fig. 4 appear hexagonal, however, the internal cells are duodecagons.

Figure 5 shows the normal stress in the x direction σ_{xx} at point C at $t = \infty$, in practice at 30 hrs, against the number of nodes across CD. The number of nodes in the x direction also changed such that the aspect ratio of the triangular elements was one. Figure 5 shows that the convergence rate of the CVFE solution is greater than that of the finite element numerical solution regardless of mesh size. For a given mesh density, the CVFE solution lies closer to the analytic solution.

Figure 6 shows the direct stress in the x direction σ_{xx} across the section CD at 2 hrs for both a coarse and a fine linear triangular finite element mesh. The coarse mesh contains

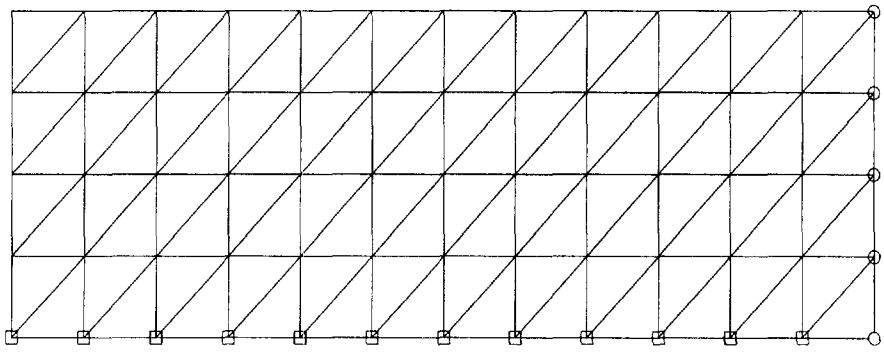

Fig. 3. Finite element linear triangular mesh.

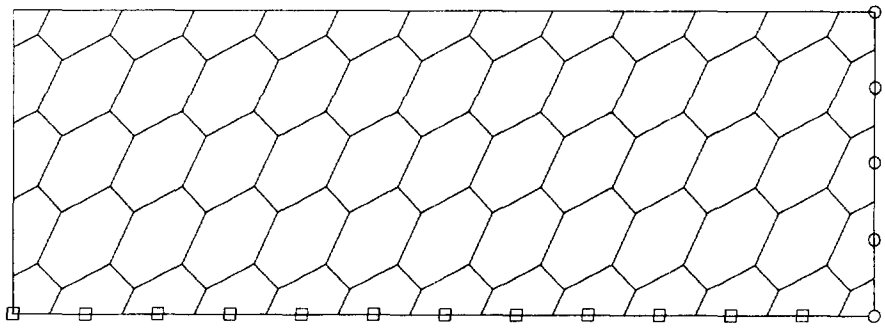

Fig. 4. Control volume computational mesh.

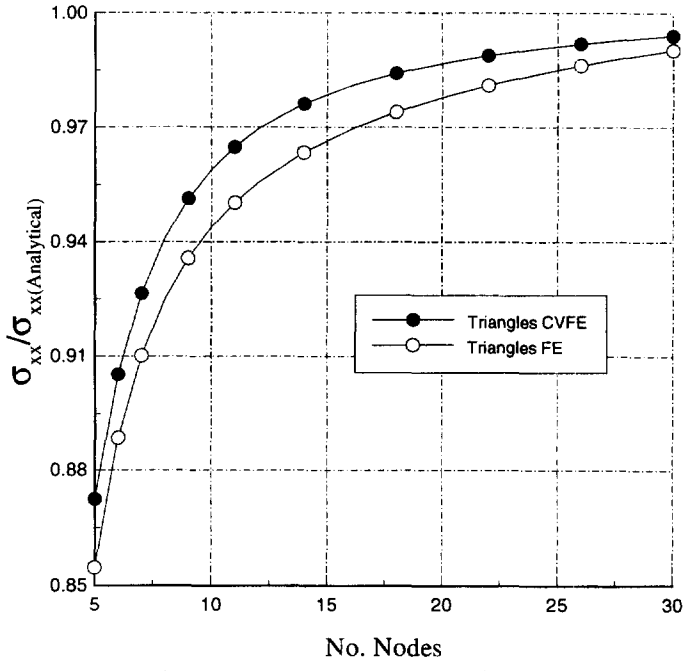

Fig. 5. Direct stress σ_{xx} at point C vs no. nodes across CD.

5 nodal points in the x direction whereas the fine mesh contains 12 nodal points. The numerical solutions are compared against the cross-section of σ_{xx} obtained from the analytical solution. In both cases, the error in the CVFE solution is smaller than that in the finite element solution. The difference between the CVFE solution, on a fine mesh, is almost indistinguishable from the analytic solutio, whereas, there is a discernable error in the finite element solution.

The direct stress in the x direction at point C against time is shown in Figure 7 for both coarse and fine meshes. In both cases, the error is smaller in the CVFE solution than that for the finite element numerical solution. The results presented in this section indicate that the control volume finite element numerical solution technique attains a greater accuracy than the finite element method for creep problems using linear triangular elements. The reason for this is that the CVFE method is conservative across each control volume, i.e. the forces are balanced at the cell level, whereas the finite element method is globally conservative.

Drying stresses

This example concerns drying induced stresses in softwoods. The timber under consideration is pine having dimensions of 160 mm × 40 mm in the radial and transverse directions respectively, Fig. 8. The timber section is symmetrical about the centrelines of

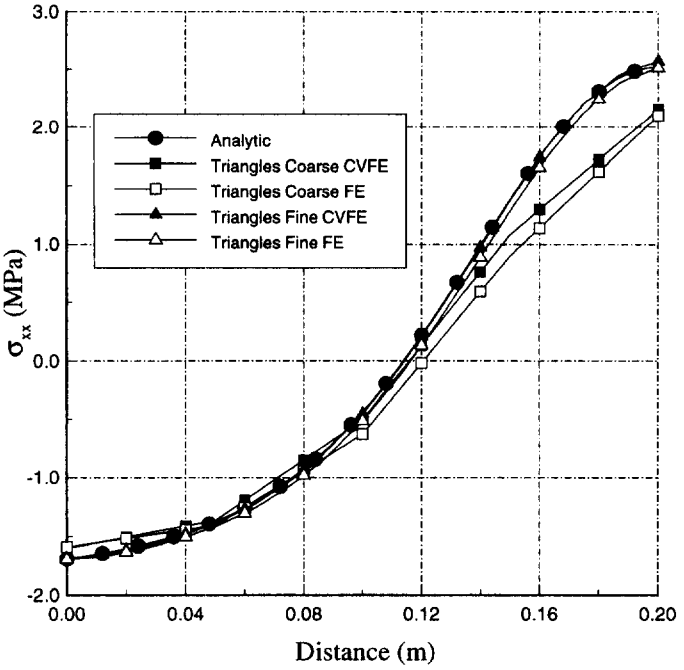

Fig. 6. Section through the stress profile σ_{xx} across CD at 2 hrs.

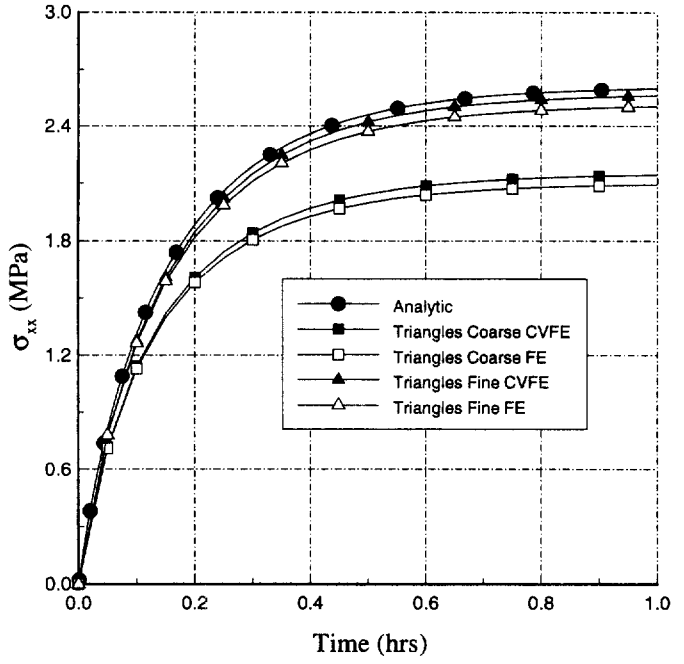

Fig. 7. Direct stress σ_{xx} at point C vs time.

both axes, therefore, only a quarter section ABCD, having dimensions 80 mm × 20 mm, need be analysed numerically.

The timber is dried by the forced convection of hot air over the exchange surfaces, faces AB and AD, across which heat is supplied and moisture evaporates into the airstream. The airstream has a velocity of 2 m/s, dry bulb temperature 120°C and wet bulb temperature 80°C. The heat and mass fluxes across the symmetry planes, faces BC and CD, are assumed to be zero. Initial conditions throughout the timber are temperature 30°C, moisture content 70% and pressure 1 bar. The thermophysical properties can be found in Perre and Degiovanni (1990). A drying model is employed to solve for the system variables of moisture

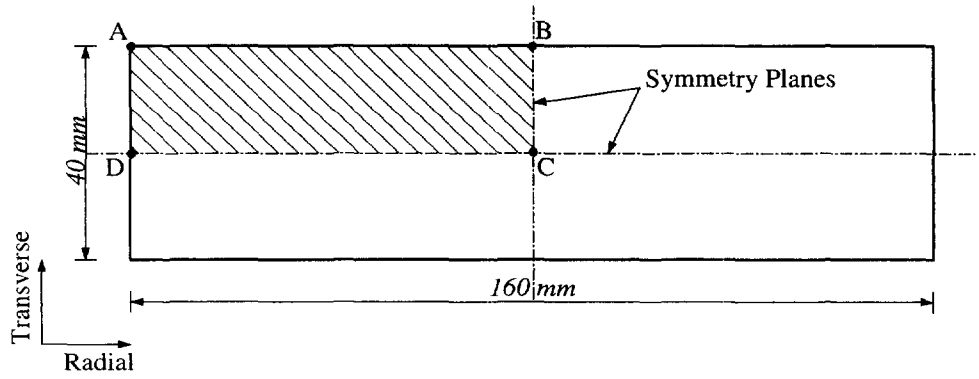

Fig. 8. Cross-section through timber sample.

content, temperature and pressure. The emphasis of this paper is on the application of the control volume finite element method to creep in softwoods during drying, hence, the drying model will not be discussed but details can be found in Ferguson (1995) and Ferguson and Turner (1995b). The moisture content, also known as the *dry basis* moisture content is the mass of water divided by the mass of the dry solid and has units of kg/kg, is defined as,

$$X = \begin{cases} X_{wf} + X_{fsp} & \text{if } X > X_{fsp} \\ X_{wb} & \text{if } X < X_{fsp} \end{cases} \tag{30}$$

where X_{wf}, X_{wb} and X_{fsp} denote the free water, bound water and fibre saturation (typically 30%) moisture content respectively. In timber drying, the free-shrinkage and creep are known to be directly proportional to the change in the bound water. Therefore, for this example, ϕ, eqns 10 and 11, denotes the bound water X_{wb}.

A numerical solution is obtained by solving the system of partial differential equations which govern the drying process, Ferguson (1995), which yields a converged solution for the system variables throughout the domain of interest. This solution can be advanced in time by employing a suitable time marching scheme. The converged solution, at the end of each timestep, is then utilised to determine the mechanical load. The solution to the drying problem is independent of stress and the drying/stress analysis coupling is through the deformed grid which is then employed for the next timestep of the drying procedure.

Material properties of the pine are Young's Modulus $E = 5 \times 10^8$ Pa, coefficient of thermal expansion $\alpha = 0.15\,^{\circ}\mathrm{C}^{-1}$, Poisson's ratio $\nu = 0.25$ and the creep coefficient $m = 0.05 \times 10^{-6}\ \mathrm{Pa}^{-1}$. Plane strain is assumed.

The finite element mesh, Fig. 9 is comprised of 432 linear triangular elements exhibiting a refinement in the region of point D. The same mesh is used in both the drying and stress models and this refinement is required to accurately model the steep moisture content gradients which arise in this region. The control volume mesh, Fig. 10, which is constructed from the finite-element mesh, contains 250 polygonal cells. The internal cells are duo-decagons whilst boundary cells are octagonal. For both meshes, nodes on face BC are restrained in the radial direction, nodes on face CD are restrained in the transverse direction and node C is restrained in both the radial and transverse directions.

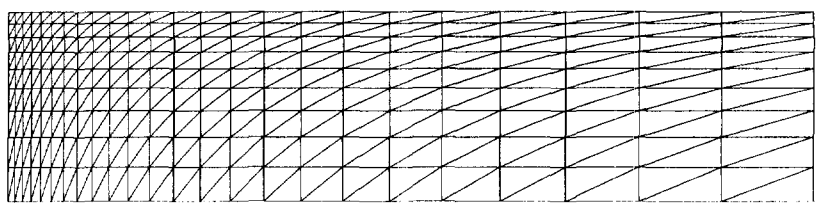

Fig. 9. Finite element linear triangular mesh.

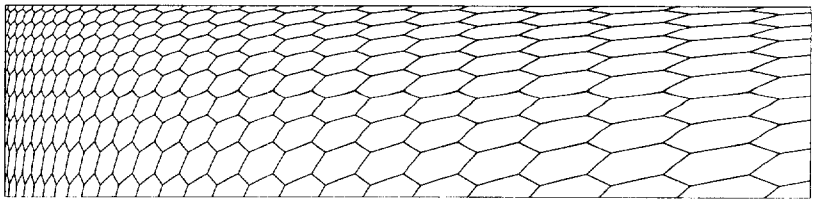

Fig. 10. Control volume computational mesh.

The variation of the moisture content within the board is two-dimensional, with steep gradients developing close to the exchange surfaces, thus, inducing two-dimensional drying stresses. Due to the complex nature of the boundary conditions across the exchange surfaces and the tight coupling of the governing partial differential equations, no analytical solution to the change in bound water in space and time exists. Therefore, no analytical solution to the evolution of stress exists.

Figure 11 presents the variation of the major principal stress vs time at points B and C. Point B lies on an exchange surface, hence, the moisture content rapidly falls below the fibre saturation point. The surface is restrained from contracting by the middle section of the wood and a tensile stress develops at the surface which is balanced by a compressive stress at the inner wetter section. As the drying process proceeds a compressive force develops in the outer sections caused by the restraint on the inner section. The reverse holds for point C, whereby, initially a compressive stress develops which changes to a tensile stress during the latter stages of drying. This behaviour is known as *stress reversal*. The CVFE and finite element numerical solutions both show the same characteristics with only minor differences being evident.

Figure 12 depicts the maximum tensile and compressive stresses which occur at any point within the timber specimen vs time. Again both numerical solutions exhibit the same characteristics. The finite element method underpredicts both the maximum tensile stress and the maximum compressive stress when compared against the CVFE solution. Industrial drying practitioners are concerned about checks or cracks developing within the dried

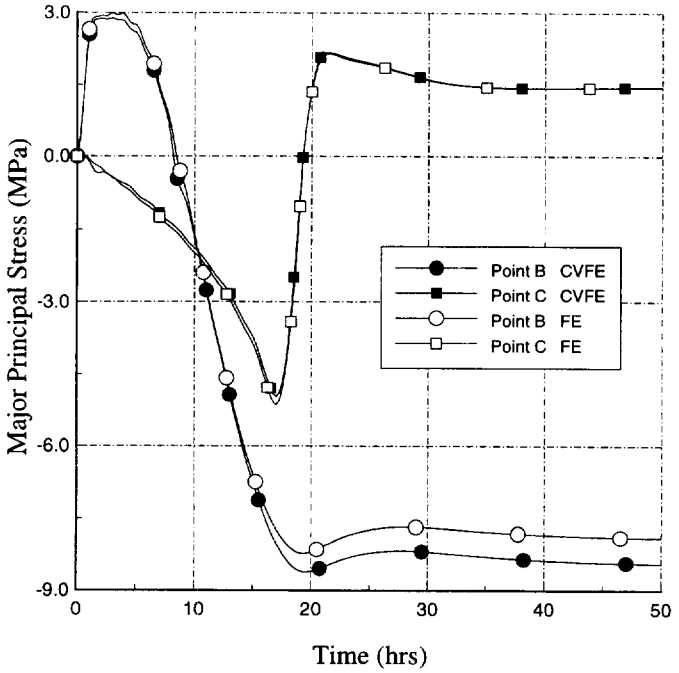

Fig. 11. Major principal stress vs time for points B and C.

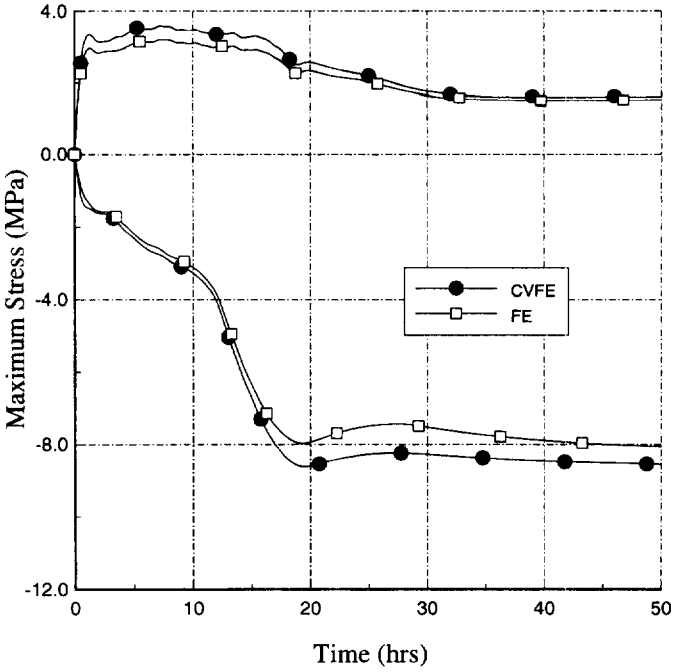

Fig. 12. Maximum tensile and compressive stress vs time.

product. A crack develops if the tensile stress exceeds the ultimate tensile strength of the wood, therefore, the discrepancy between the two solutions between 2 and 15 hrs is of concern.

Industrial drying practitioners are also concerned with the straightness of the dried board. Figure 13 shows the deformation of point D vs time. Although the trends of both numerical solutions are the same, the finite element method overpredicts the deformation in the radial and transverse directions when compared against the CVFE solution.

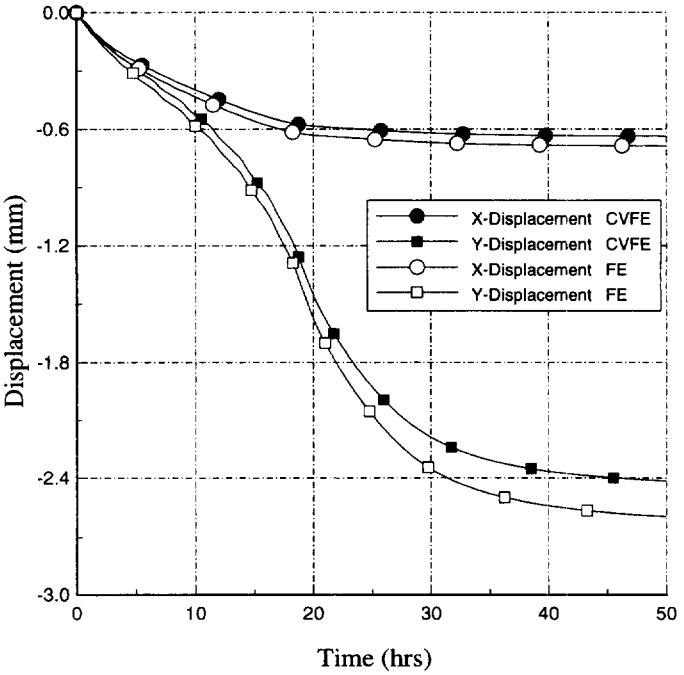

Fig. 13. Nodal displacement of point A.

CONCLUSIONS

The results presented in this paper show that the control volume finite element numerical solution technique is a valid, effective and robust tool to be employed in solving creep problems. The CVFE discretisation which has been presented is valid to both structured and unstructured meshes without alteration to the formulation. Two problems were presented, firstly, a beam was subjected to a known temperature variation in time and space, and secondly, drying induced stresses in timber were calculated.

The CVFE and finite element numerical solutions exhibited the same trends for the drying stress problem. However, the finite element method underpredicted the stresses whilst overpredicted the displacements within the timber sample in comparison to the CVFE results. In the softwood drying industry, quality of the final dried product is a major concern. Wastage through excessive cracking accounts for approximately 8% of the total volume throughput. Therefore, if the coupled drying/stress model is to be incorporated into a design tool for timber drying practitioners, one must err on the side of caution.

Both numerical solutions displayed the same characteristics for the beam problem. This problem was subject to a one-dimensional temperature variation in order to solve the problem analytically. The CVFE method proved to be more accurate for all the linear triangular meshes used with total nodes ranging from 60 to 2250. The CVFE method is locally conservative, in that the forces are balanced around each control volume whereas the finite element method is globally conservative. High ordered control volumes, duodecagons, are constructed from the linear triangular finite element mesh which leads to a smaller conservation error across each cell than if, for instance, pentagons were employed. This coupled with the fact that a one point Radua integration rule was used in the finite element method accounts for the difference. Future work includes comparing the CVFE and FE methods for a linear quadrilateral mesh from which an octagonal control volume mesh is derived.

REFERENCES

Andrade, E. N. da C. (1910) The viscous flow of metals and allied phenomena. *Proceedings of the Royal Society* **84.**

Bailey, C. and Cross, (1995) A finite volume procedure to solve elastic solid mechanics problems in three dimensions on an unstructured mesh. *International Journal of Numerical Methods in Engineering* **38,** 1757–1776.

Bailey, C., Fryer, Y. D., Cross, M. and Chow, P. (1993) Predicting the deformation of castings in moulds using a control volume approach in unstructured meshes. In *Mathematical Modelling for Material Processing*, eds Cross, M. *et al.*, pp. 259–272. Oxford University Press, U.K.

Boley, B. A. and Weiner, J. H. (1960) *Theory of Thermal Stresses*. John Wiley and Sons, Inc, New York.

Duxbury, P., Crook, T. Lyons, P. (1994) A consistent formulation for the integration of combined plasticity and creep. *International Journal of Numerical Methods in Engineering* **37,** 1277–1295.

Ferguson, W. J. (1995) A control volume finite element numerical simulation of the high temperature drying of spruce. *Drying Technology* **13,** 607–634.

Ferguson, W. J. and Turner, I. W. (1995a) A study of two-dimensional cell-centred and vertex-centred control volume schemes applied to high temperature timber drying. *Numerical Heat Transfer Part B: Fundamentals* **27,** 393–415.

Ferguson, W. J. and Turner, I. W. (1995b) A comparison of the finite element and control volume numerical solution techniques applied to timber drying problems below the boiling point. *International Journal of Numerical Methods in Engineering* **38,** 451–467.

Fung, L. S., Hiebert, A. D. and Nghiem. L. X. (1992) Reservoir simulation with a control-volume finite-element method. *SPE Reservoir Engineering* **15,** 349–357.

McVetty, P. G. (1934) Working stresses for high temperature service. *Mechanical Engineering* **56.**

McVetty, P. G. (1943) Creep of metals at elevated temperatures—the hyperbolic sine relation between stress and creep rate. *Transactions ASME* **65,** .

Norton, F. H. (1929) *The Creep of Steel at High Temperatures*. McGraw-Hill, New York.

Onate, E., Cervera, M. and Zienkiewicz, O. (1994) A finite volume format for structural mechanics. *International Journal of Numerical Methods in Engineering* **37,** 181–201.

Patankar, S. V. (1980) *Numerical Heat Transfer and Fluid Flow*. McGraw-Hill, New York.

Perre, P. and Degiovanni, A. (1990) Simulation par volumes finis des transferts couples en milieu poreux anisotrope: sechage de bois a basse et a haute temperature. *International Journal of Heat Mass Transfer* **33,** 2463–2478.

Ranta-Maunus, A. (1975) The viscoelasticity of wood at varying moisture contents. *Wood Science Technology* **9,** 189–205.

Taylor, G., Bailey, C. and Cross, (1995) Solution of elastic visco-plastic equations: A finite volume approach. *Applied Mathematical Modelling* (accepted).

Turner, I. W. and Ferguson, W. J. (1995a) An unstructured mesh cell-centred control volume method for simulating heat and mass transfer in porous media: Application to softwood drying. Part I: The isotropic model. *Applied Mathematical Modelling* **19,** 654–667.

Turner, I. W. and Ferguson, W. J. (1995b) An unstructured mesh cell-centred control volume method for simulating heat and mass transfer in porous media: Application to softwood drying. Part II: The anisotropic model. *Applied Mathematical Modelling* **19,** 668–674.

Zienkiewicz, O. C. (1977). *The Finite Element Method.* MacGraw-Hill, London.

Zienkiewicz, O. C. and Cormeau, I. C. (1974) Visco-plasticity—plasticity and creep in elastic solids—a unified numerical solution approach. *International Journal of Numerical Methods Engineering* **8,** 821–845.